The Plant Cell, Vol. 27: 2926–2940, October 2015, www.plantcell.org

CELLULOSE SYNTHASE INTERACTIVE1 Is Required for Fast Recycling of Cellulose Synthase Complexes to the Plasma Membrane in Arabidopsis

Lei Lei,[a] Abhishek Singh,[b] Logan Bashline,[a] Shundai Li,[a] Yaroslava G. Yingling,[b] and Ying Gu[a,1]

[a] Department of Biochemistry and Molecular Biology, Pennsylvania State University, University Park, Pennsylvania 16802
[b] Department of Materials Science and Engineering, North Carolina State University, Raleigh, North Carolina 27695

ORCID IDs: 0000-0002-9450-7229 (A.S.); 0000-0002-8557-9992 (Y.G.Y.); 0000-0001-8415-4768 (Y.G.)

Plants are constantly subjected to various biotic and abiotic stresses and have evolved complex strategies to cope with these stresses. For example, plant cells endocytose plasma membrane material under stress and subsequently recycle it back when the stress conditions are relieved. Cellulose biosynthesis is a tightly regulated process that is performed by plasma membrane-localized cellulose synthase (CESA) complexes (CSCs). However, the regulatory mechanism of cellulose biosynthesis under abiotic stress has not been well explored. In this study, we show that small CESA compartments (SmaCCs) or microtubule-associated cellulose synthase compartments (MASCs) are critical for fast recovery of CSCs to the plasma membrane after stress is relieved in *Arabidopsis thaliana*. This SmaCC/MASC-mediated fast recovery of CSCs is dependent on CELLULOSE SYNTHASE INTERACTIVE1 (CSI1), a protein previously known to represent the link between CSCs and cortical microtubules. Independently, AP2M, a core component in clathrin-mediated endocytosis, plays a role in the formation of SmaCCs/MASCs. Together, our study establishes a model in which CSI1-dependent SmaCCs/MASCs are formed through a process that involves endocytosis, which represents an important mechanism for plants to quickly regulate cellulose synthesis under abiotic stress.

INTRODUCTION

Much of our current understanding of endocytosis has been deduced from yeast and animal systems, where cells internalize ligands, surface receptors, extracellular material, and membrane material by endocytosis. In some striking examples, such as fibroblasts, it is estimated that the equivalent of 50% of the cell surface is internalized per hour and replenished by secretion and recycling processes (Steinman et al., 1983). In many cases, internalized cell surface materials are recycled back to the cell surface. The balance between endocytosis and recycling is an important mechanism that regulates diverse cellular processes such as cytokinesis (Albertson et al., 2005), cell junction formation (Chalmers and Whitley, 2012), polarity establishment (Eaton and Martin-Belmonte, 2014), and integrin signaling (Wickström and Fassler, 2011). While endocytosis and recycling networks have been extensively characterized in mammalian cells, endocytosis and recycling were largely overlooked in plants for some time because of the false notion that endocytosis is suppressed under the high turgor pressure that pushes the plasma membrane (PM) tightly against the cell walls of plant cells. It is now known that endocytosis and recycling play important roles in cell wall remodeling, gravitropism, pathogen defense, guard cell movement, and hormone signaling in plants (Samaj et al., 2005). Recently, many clathrin-mediated endocytosis (CME) components and cargo proteins have been identified and characterized in *Arabidopsis thaliana* (Konopka et al., 2008; Van Damme et al., 2011; Ito et al., 2012; Song et al., 2012; Bashline et al., 2013; Di Rubbo et al., 2013; Fan et al., 2013; Kim et al., 2013; Wang et al., 2013; Yamaoka et al., 2013; Gadeyne et al., 2014). One particular cargo protein, cellulose synthase (CESA), acts as a unique anchor that can be used to dissect endocytic uptake and recycling pathways in plants (Bashline et al., 2013, 2014a).

CESAs are part of multimeric protein complexes that are often referred to as the cellulose synthase complexes (CSCs), which are responsible for synthesizing cellulose at the PMs of plant cells. Nascent cellulose microfibrils are extruded from the CSCs into the apoplast, where they are incorporated into the cell wall and serve a major loading-bearing role (Somerville, 2006; Li et al., 2014). CSCs are presumed to only synthesize cellulose when they are localized to the PM, where the force of cellulose polymerization drives the motility of CSCs laterally through the plane of the PM. The trajectories of CSC motility coalign with cortical microtubules, which run along the cytoplasmic surface of the PM (Paredez et al., 2006). CELLULOSE SYNTHASE INTERACTIVE1 (CSI1) is required not only for the coalignment of active CSCs and cortical microtubules, but also for CSCs to efficiently synthesize cellulose (Gu et al., 2010; Bringmann et al., 2012; Li et al., 2012).

In addition to the PM, CSCs have also been shown to localize to the Golgi apparatus, to the *trans*-Golgi network (TGN), and to early endosomes (EEs) by multiple techniques, including electron microscopy, immunogold labeling, and live-cell imaging of fluorescent protein-tagged CESAs (Haigler and Brown, 1986; Paredez et al., 2006; Crowell et al., 2009; Gutierrez et al., 2009). A recent proteomic analysis revealed that CESA proteins are likely present in SYP61-labeled vesicles (Drakakaki et al., 2012; Worden et al.,

[1] Address correspondence to yug13@psu.edu.
The author responsible for distribution of materials integral to the findings presented in this article in accordance with the policy described in the Instructions for Authors (www.plantcell.org) is: Ying Gu (yug13@psu.edu).
www.plantcell.org/cgi/doi/10.1105/tpc.15.00442

2012). SYP61 is a Q-SNARE that has overlapping localization in the TGN and EE, which is believed to be a single compartment in plants containing both secretory and endocytic materials (Viotti et al., 2010). Therefore, CESA signals in the TGN/EE could be part of the de novo secretion pathway, the endocytic pathway, or a recycling pathway (Bashline et al., 2014a). Although CSCs have been detected in the Golgi and TGN/EE, the prerequisite that CSCs must be localized at the PM to synthesize cellulose has propelled the study of the delivery and endocytosis of CSCs at the PM. Genetic data suggest that CME represents at least one mechanism for CSC internalization. Mutations in dynamin-related proteins in both rice (*Oryza sativa*; *brittle culm3*) and Arabidopsis (*radial swelling9*) exhibit endocytic defects and a reduction in cellulose content, but a direct connection between dynamin-related proteins and CSC endocytosis has not been demonstrated (Collings et al., 2008; Xiong et al., 2010). More recently, multiple lines of evidence have suggested that CESA is a cargo of the CME pathway. CESA was shown to directly interact with AP2M (previously referred to as μ2), the medium subunit of the AP2 complex, which participates in recruiting cargo proteins and the clathrin machinery to the sites of CME (Jackson et al., 2010; Cocucci et al., 2012). Loss of AP2M in *ap2m-1* (previously referred to as *μ2-1*) caused an increase in CESA abundance at the PM in interphase cells, providing evidence that CME regulates CESA distribution at the PM (Bashline et al., 2013). Clathrin-mediated retrieval of CSC was also observed in the developing cell plate (Miart et al., 2014). It is not known whether the internalized CESAs are degraded or recycled. It is tempting to hypothesize that plant cells would recycle the CSC due to the energy cost of synthesizing a protein complex as large as the CSC (Bashline et al., 2014a).

Another population of CSC-containing vesicles, referred to as small CESA compartments (SmaCCs) or microtubule-associated cellulose synthase compartments (MASCs), is often associated with cortical microtubules at the cell periphery near the PM (Crowell et al., 2009; Gutierrez et al., 2009). SmaCCs/MASCs are frequently observed in epidermal cells at the base of hypocotyl, where the density of PM-localized CSCs is low and the cells have slowed their expansion. Osmotic stress or treatment with isoxaben, a cellulose synthesis inhibitor, has been shown to deplete the PM-localized CSC population and to reveal or induce SmaCC/MASC formation. The function of SmaCCs/MASCs is unclear. SmaCCs/MASCs are likely delivery compartments or intracellular storage vesicles of internalized CSCs (Crowell et al., 2009; Gutierrez et al., 2009). In addition to CESA proteins, CSI1 and CSI3 have also been shown to be associated with SmaCCs/MASCs (Lei et al., 2012, 2013). CSI3 exhibits many CSI1-like characteristics, such as the ability to interact with CESAs and colocalize with CESAs at the PM and in SmaCCs/MASCs. However, CSI3 is dispensable for the coalignment between CESA and microtubules and plays a distinct role in cellulose synthesis that is dependent on the function of CS1 (Lei et al., 2013).

In this study, we showed that in addition to linking CSCs to microtubules during cellulose biosynthesis, CSI1 is also important for the formation of SmaCCs/MASCs under stress conditions. Furthermore, CSI1-dependent SmaCCs/MASCs are critical for the fast recovery of CSCs to the PM after relief from stress conditions. Inhibition of endocytosis by pharmacological or genetic means reduced the accumulation of SmaCCs/MASCs under stress conditions. Together, these observations suggest that CSI1-dependent SmaCCs/MASCs may act as recycling compartments under stress conditions and are formed through a process that involves endocytosis. Domain analysis and 3D structure prediction of CSI1 protein establish the hypothesis that the armadillo (ARM) repeats of CSI1 are involved in CSI1-CESA interactions and that the C2 domain of CSI1 has multiple functions in CSI1 targeting, microtubule binding, CESA binding, and SmaCC/MASC formation. Therefore, CSI1 plays multiple roles in the regulation of cellulose biosynthesis.

RESULTS

The C2 Domain of CSI1 Interacts with CESA and Microtubules

Previous studies have shown that CSI1 is a microtubule binding protein that is required for the coalignment between CSCs and microtubules (Gu et al., 2010; Li et al., 2012). To determine which domain of CSI1 is required for the interaction with microtubules, we generated several truncations of CSI1 (Figure 1A). The 6×His-tagged CSI1 truncations were heterologously expressed in *Escherichia coli* and affinity-purified proteins were used in the in vitro microtubule binding assay. Full-length CSI1 and CSI1$^{2012\text{-}2150}$ interacted with microtubules strongly, similar to the positive control, MICROTUBULE-ASSOCIATED PROTEIN2 (MAP2) (Figure 1B). CSI1$^{1\text{-}577}$ and CSI1$^{1738\text{-}2150}$ each showed weak microtubule binding capability (Figure 1B). CSI1$^{1\text{-}2013}$, CSI1$^{1\text{-}1737}$, CSI1$^{1\text{-}998}$, and CSI1$^{1793\text{-}1899}$ did not interact with microtubules, similar to the negative control, BSA (Figure 1B). Both CSI1$^{1738\text{-}2150}$ and CSI1$^{2012\text{-}2150}$ contain the C-terminal C2 domain of CSI1 and both interact with microtubules. Compared with CSI1$^{2012\text{-}2150}$, CSI1$^{1738\text{-}2150}$ contains two additional ARM repeats. However, a truncation containing only those two ARM repeats, CSI1$^{1793\text{-}1899}$, did not bind to microtubules. Together, these data suggest that the C2 domain of CSI1 plays a part in microtubule binding. We further determined the affinity of CSI1$^{2012\text{-}2150}$ for microtubules by a saturation binding assay where a constant concentration of taxol-stabilized microtubules was incubated with a gradient of CSI1$^{2012\text{-}2150}$ concentrations. The dissociation constant of CSI1$^{2012\text{-}2150}$ was ~0.52 ± 0.14 μM (Supplemental Figure 1), which is comparable to the dissociation constant of full-length CSI1 (Li et al., 2012).

In planta, CSI1 not only interacts with cortical microtubule, but it also binds CESA (Gu et al., 2010). CSI1 has been previously shown to interact with CESAs in a yeast two-hybrid assay (Gu et al., 2010; Lei et al., 2013). However, the direct interaction between purified full-length CSI1 protein and CESA protein has not been established in vitro. GST (glutathione *S*-transferase)-tagged central domains of CESA1 and CESA3 (GST-CESA1CD and GST-CESA3CD) were affinity purified and used in in vitro pull-down experiments with the 6×His-tagged full-length CSI1 and the CSI1 truncations. The GST tag alone served as the negative control and was unable to interact with any of the CSI1 proteins (Supplemental Figure 2). GST-CESA1CD and GST-CESA3CD were able to pull down full-length CSI1 protein and multiple truncated fragments of CSI1, indicating that the interaction between CESA and CSI1 occurs at

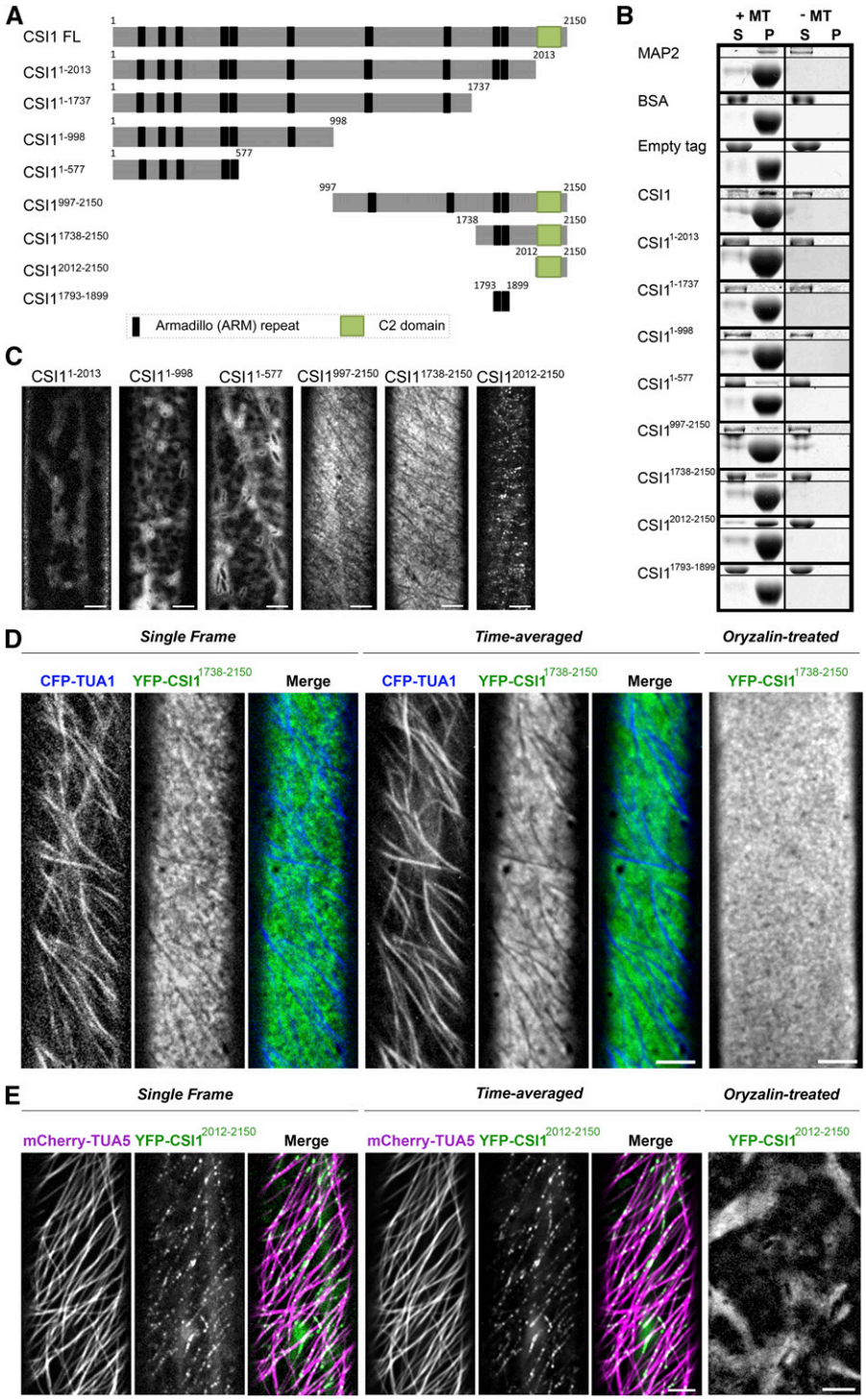

Figure 1. The C Terminus of CSI1 Is Required for Microtubule Binding in Vitro and Colocalization with Microtubules in Vivo.

(A) Schematic diagram of the CSI1 full-length protein (CSI1 FL) and different truncations. Black bars represent predicted ARM repeats, and green boxes represent the C2 domain.

(B) C2 domain binds to microtubules in vitro. Equal amounts of His-tagged proteins were used in the presence (+) or absence (−) of taxol-stabilized microtubules (MTs). MAP2 was used as a positive control. BSA and empty tag were used as negative controls. For each microtubule binding experiment, representative gels from three technical replicates are shown. Upper panel shows purified proteins, and lower panel shows tubulin. S, supernatant; P, pellet.

multiple sites. CSI1$^{1793-1899}$ and CSI1$^{2012-2150}$ were among the shortest truncated fragments of CSI1 that interacted with CESAs, suggesting that the C2 domain and/or ARM repeats of CSI1 can potentially mediate the interaction between CSI1 and CESAs. Interestingly, GST-CESA1CD and GST-CESA3CD was able to pull down CSI1$^{1-577}$ but not CSI1$^{1-1737}$ and CSI1$^{1-2013}$, even though all three have multiple ARM repeats. A possible scenario is that the interaction between CESACD and CSI1 truncations might require a proper external surface and the external surface of the CSI1$^{1-1737}$ and CSI1$^{1-2013}$ might be disrupted by intramolecular inhibition. Consistent with this hypothesis, CSI1$^{1-577}$ was able to bind microtubules in vitro, but not CSI1$^{1-1737}$ or CSI1$^{1-2013}$.

To further investigate the function of CSI1 protein domains, we assessed the subcellular localization of YFP-tagged CSI1 truncations in transgenic Arabidopsis seedlings. Each of the YFP-tagged CSI1 truncations was driven by the 35S promoter. Their localization could be classified into three different types: intracellular diffuse signals (CSI1$^{1-2013}$, CSI1$^{1-998}$, and CSI1$^{1-577}$), PM-localized signals (CSI1$^{997-2150}$ and CSI1$^{1738-2150}$), or distinct puncta at the cell cortex (CSI1$^{2012-2150}$; Figure 1C). The localization of CSI1$^{997-2150}$ and CSI1$^{1738-2150}$ appeared to be identical; therefore, YFP-CSI1$^{1738-2150}$ was used for further analysis. Twenty minutes of exposure to FM4-64, a membrane-impermeable fluorescent lipid dye, was used to label the PM to determine the focal plane of YFP-CSI1$^{1738-2150}$ and YFP-CSI1$^{2012-2150}$ (Bolte et al., 2004). YFP-CSI1$^{1738-2150}$ colocalized with FM4-64 at the focal plane of the PM, whereas YFP-CSI1$^{2012-2150}$ localized to puncta adjacent to the PM at the cell cortex (Supplemental Figure 3). YFP-CSI1$^{1738-2150}$ localized with a uniform distribution at the PM, with the exception of multiple linear stripes that lacked fluorescence and were reminiscent of cortical microtubules. To verify the identity of these stripes, we generated Arabidopsis seedlings coexpressing CFP-TUA1 (ALPHA-1 TUBULIN) and YFP-CSI1$^{1738-2150}$. CFP-TUA1 labeled the stripes that were devoid of YFP-CSI1$^{1738-2150}$ signal (Figure 1D; Supplemental Movie 1). Furthermore, treatment with oryzalin, a microtubule depolymerization reagent, removed the stripes, which resulted in a uniform distribution of YFP-CSI1$^{1738-2150}$ at the PM (Figure 1D). In contrast, YFP-CSI1$^{2012-2150}$, which is representative of the CSI1 C2 domain, localized to small cortical compartments along linear tracks that were reminiscent of cortical microtubules (Figure 1C). In the Arabidopsis seedlings coexpressing mCherry-TUA5 and YFP-CSI1$^{2012-2150}$, YFP-CSI1$^{2012-2150}$ colocalized with cortical microtubules extensively (Supplemental Movie 2). Oryzalin treatment depleted most of the cortical YFP-CSI1$^{2012-2150}$ punctate signals, suggesting that the particles were connected with the cortical microtubules (Figure 1E; Supplemental Movie 3). Therefore, the in vivo localization of both YFP-CSI1$^{1738-2150}$ and YFP-CSI1$^{2012-2150}$ is influenced by cortical microtubules.

The C2 domain of CSI1 is capable of interacting with both CESA and microtubules and localized to cortical microtubules when expressed in vivo. To further illustrate the importance of the C2 domain, loss of the C2 domain in YFP-CSI1$^{1-2013}$ disrupted the subcellular localization of CSI1 in vivo (Figure 1C) and abolished the interaction between His-CSI1$^{1-2013}$ and microtubules or CESAs in vitro (Figure 1B; Supplemental Figure 3). Furthermore, truncated CSI1 that lacked the C2 domain was not able to rescue the phenotype of the *csi1-6* mutant (Supplemental Figure 4), suggesting that the C2 domain is essential for the function of CSI1 in Arabidopsis.

Modeling of CSI1

In the absence of an experimentally determined structure of CSI1 protein, a protein structure prediction method similar to one used for the prediction of the plant CESA model structure was applied (Sethaphong et al., 2013). The model structure of CSI1 protein was based on a combination of secondary structure prediction (PSIPRED; Supplemental Figure 5), a template-based protein prediction server (RaptorX; Supplemental Table 1), and molecular dynamics (MD) simulations (Supplemental Figure 6). The secondary structure prediction revealed that CSI1 consists largely of α-helixes and some β-sheets at the N and C termini (Supplemental Figure 5). The three-dimensional model structure of CSI1 showed that the central domain forms contiguous α-helical layers that are arranged into a long loop-like ribbon structure with the C2 domain that folds into β-sheets (Figure 2A). MD simulations indicated that free CSI1 has considerable flexibility in solution, while maintaining stable alpha helical arrangements (Supplemental Figure 6). As determined in this study, the loop-like structure of CSI1 has several CSC binding sites and also interacts with microtubules (Figure 2A). A putative interaction mode of CSI1 with the CSC and microtubule was simulated such that the CSI1 protein was in bended loop-like conformation (as depicted in Figure 2), with its central domain binding to the CSC and N and C termini interacting with microtubules, which is consistent with the in vitro interaction data obtained using the CSI1 truncations.

The C2 Domain of CSI1 Colocalizes with SmaCCs

Although the majority of YFP-CSI1$^{2012-2150}$ labeled cortical compartments were immobile (Supplemental Movie 4), a few of them displayed microtubule-shrinking end tracking behaviors

Figure 1. (continued).

(C) YFP-tagged CSI1 truncations are localized to different compartments in vivo. Arabidopsis seedlings expressing YFP-tagged CSI1 truncations were grown in the dark for 3 d before imaging. Single optical sections in epidermal cells ~2 mm below the apical hook were imaged by confocal microscopy. Bars = 5 μm.

(D) YFP-CSI1$^{1738-2150}$ localizes at PM excluding underlying microtubules. Arabidopsis seedlings coexpressing YFP-CSI1$^{1738-2150}$ and CFP-TUA1 were imaged by confocal microscopy. Single optical sections, time average of 61 frames (2-min duration; 2-s interval), and merged images are shown. YFP-CSI1$^{1738-2150}$ lost its distinct localization after 5 h treatment with 20 μM oryzalin. Bars = 5 μm.

(E) YFP-CSI1$^{2012-2150}$ colocalizes with cortical microtubules. Single optical sections, time average of 61 frames (2-min duration; 2-s interval), and merged images of seedlings coexpressing YFP-CSI1$^{2012-2150}$ and mCherry-TUA5 are shown. YFP-CSI1$^{2012-2150}$ lost its distinct localization after 5 h of treatment with 20 μM oryzalin. Bars = 5 μm.

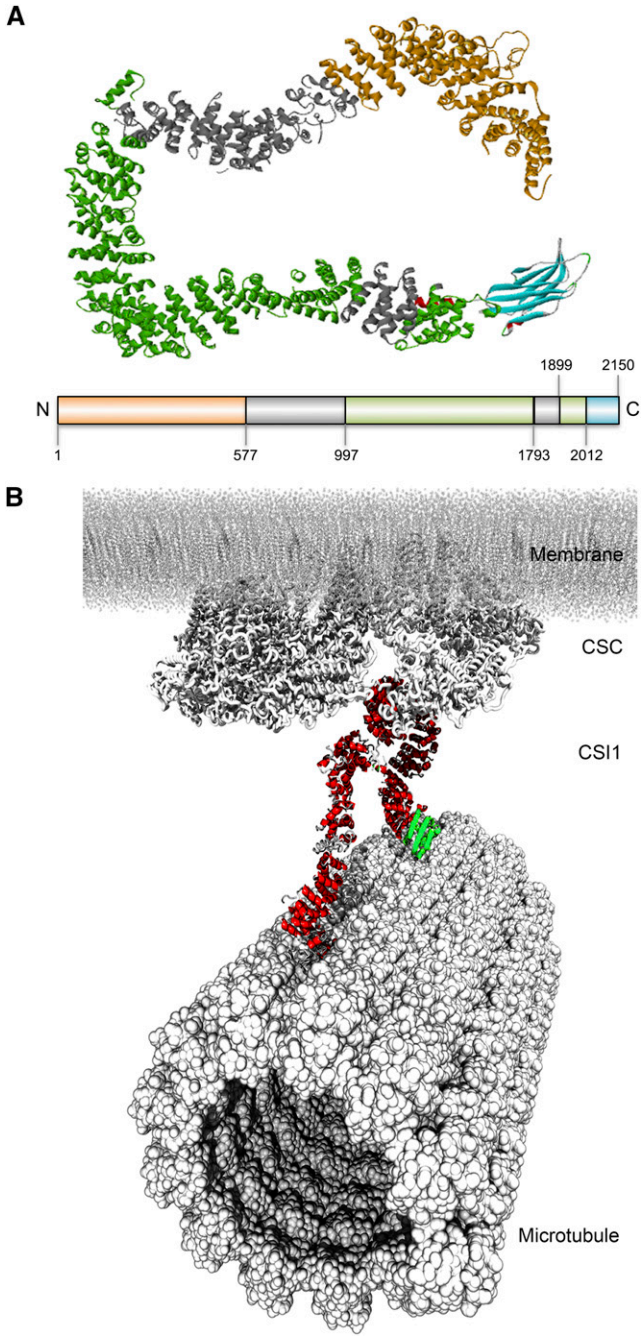

Figure 2. Computational Modeling of CSI1 Protein Structure.

(A) Model of CSI1 protein colored by regions investigated in this article and specified on the bar.

(B) Putative interaction mode of CSI1 with CSC complex and microtubule. Within CSI1 protein, the α-helices are red and the β-sheets are green.

(Supplemental Movie 5), which is similar to what has been reported for SmaCCs/MASCs (Gutierrez et al., 2009). To investigate whether YFP-CSI1$^{2012\text{-}2150}$ overlapped with SmaCCs/MASCs, we generated transgenic lines carrying both YFP-CSI1$^{2012\text{-}2150}$ and mCherry-CESA6. Upon 100 nM isoxaben treatment for 2 h, both mCherry-CESA6 and YFP-CSI1$^{2012\text{-}2150}$ accumulated in SmaCCs/MASCs (Figure 3A; Supplemental Movie 4). More YFP-CSI1$^{2012\text{-}2150}$ particles were present than mCherry-CESA6-labeled SmaCCs/MASCs, probably due to the overexpression of YFP-CSI1$^{2012\text{-}2150}$. Approximately 70% (72 out of 102) of SmaCCs/MASCs labeled with mCherry-CESA6 were colocalized with YFP-CSI1$^{2012\text{-}2150}$ particles. YFP-CSI1$^{2012\text{-}2150}$ particles had a similar velocity distribution to that of SmaCCs/MASCs labeled with mCherry-CESA6 (Figure 3B), and colocalized particles often exhibited the same movement (Figure 3C; Supplemental Movie 6). CSI1 has been previously shown to associate with CESA in SmaCCs (Bringmann et al., 2012; Lei et al., 2013). Our data indicate that the C2 domain of CSI1 might be involved in the association of CSI1 and CESA in SmaCCs/MASCs.

CSI1 Is Required for the Formation of SmaCCs/MASCs

To investigate whether CSI proteins play a role in the formation of SmaCCs/MASCs, we compared the accumulation of SmaCCs/MASCs in the wild type, *csi1*, and *csi1 csi3* mutants upon 100 nM isoxaben treatment. Mock treatment with DMSO did not affect the distribution of YFP-CESA6 in the wild type, *csi1*, or *csi1 csi3* mutants, and the density of PM-localized YFP-CESA6 was comparable in each line at ~0.9 puncta per μm^2 (Figures 4A to 4C). Upon 2 h treatment with 100 nM isoxaben, SmaCCs/MASCs accumulated in wild-type cells with an average density of ~0.1 SmaCCs/MASCs per μm^2 (Figures 4A, 4B, and 4D; Supplemental Movie 7). However, in *csi1* and *csi1 csi3*, the accumulation of SmaCCs/MASCs was barely detectable, suggesting that CSI1 plays a significant role in the formation of isoxaben-induced SmaCCs/MASCs and that CSI1 plays a dominant role in SmaCC/MASC formation over CSI3 (Figures 4A, 4B, and 4D). Consistent with the idea that CSI3 is dispensable for formation of SmaCCs/MASCs, the accumulation of isoxaben-induced SmaCCs/MASCs was not affected in the *csi3* mutant (Supplemental Figure 7).

CSI1 Is Required for the Fast Recovery of PM-Localized CSCs after Stress

To understand whether CSI1, as well as SmaCCs/MASCs, has a role in maintaining PM-localized CSCs, we examined the recovery of PM-localized CSCs after isoxaben washout. The 2.5-d-old etiolated Arabidopsis seedlings expressing YFP-CESA6 were incubated in 0.5× Murashige and Skoog (MS) liquid medium containing 100 nM isoxaben for 2 h before washout (Figure 5). Before treatment, there were comparable densities of PM-localized CSCs in both the wild type and *csi1* (before 120 min isoxaben treatment; Figures 5A to 5C). In the wild type, isoxaben treatment triggered the clearance of PM-localized CSCs and the generation of SmaCCs/MASCs (washout 0 min; Figure 5A). After washout using 0.5× MS liquid medium, the recovery of CSCs at the PM was monitored every 30 min for 180 min. For wild-type seedlings, the density increased drastically within 30 min after washout, and the density of PM-localized CSCs stabilized ~120 min after washout. However, in *csi1* mutants, no visible SmaCCs/MASCs were formed after isoxaben treatment, and the recovery of PM-localized CSCs was significantly slower compared with wild-type seedlings. At 180 min after washout, the density of PM-localized CSCs

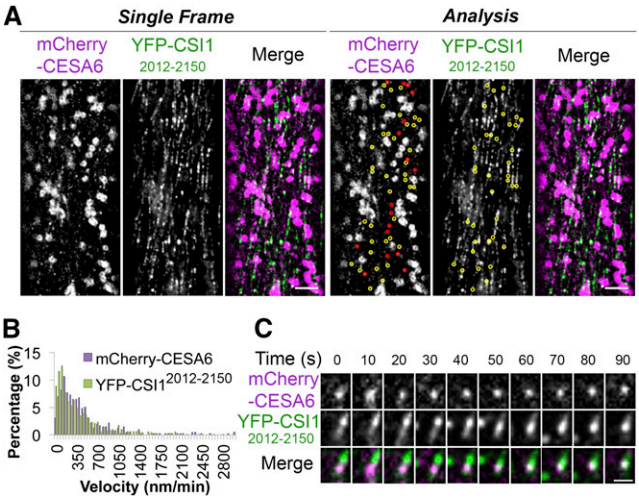

Figure 3. YFP-CSI1$^{2012\text{-}2150}$ Colocalizes with SmaCCs.

Arabidopsis seedlings coexpressing mCherry-CESA6 and YFP-CSI1$^{2012\text{-}2150}$ were treated with 100 nM isoxaben for 2 h before imaging.

(A) Two-channel single optical section of mCherry-CESA6 and YFP-CSI1$^{2012\text{-}2150}$ and colocalization analysis. Yellow circles indicate colocalized mCherry-CESA6 and YFP-CSI1$^{2012\text{-}2150}$ in SmaCCs. Red circles indicate mCherry-CESA6-labeled SmaCCs, which did not colocalize with YFP-CSI1$^{2012\text{-}2150}$. Bar = 5 μm.

(B) Histogram of particle velocities. The mean velocity is 485 ± 507 nm/min for mCherry-CESA6 (n = 413) and 441 ± 506 nm/min for YFP-CSI1$^{2012\text{-}2150}$ (n = 813).

(C) A time series of images shows dynamic behavior of colocalized YFP-CSI1$^{2012\text{-}2150}$ and mCherry-CESA6. Shown is one representative instance chosen from 72 documented events. Bar = 1 μm.

in *csi1* was still ~0.33 puncta per μm^2, accounting for only 39% of the CSC density before treatment (Figures 5A to 5C). These data suggest that CSI1 and/or CSI1-dependent SmaCCs/MASCs are important for the fast recovery of PM-localized CSCs after the removal of isoxaben.

As isoxaben pharmacologically inhibits cellulose synthesis, we sought to use an alternative stress condition to test the hypothesis that CSI1 affects the fast recovery of PM-localized CSCs. Mannitol has been previously shown to induce osmotic stress, which leads to a reduction in PM-localized CSCs and the accumulation of SmaCCs/MASCs (Crowell et al., 2009; Gutierrez et al., 2009). We repeated the washout experiments after 3 h of 200 mM mannitol treatment. Similar to isoxaben washout experiments, the recovery of PM-localized CSCs upon mannitol washout in *csi1* lagged behind that of the wild type at all time points (Figure 5; Supplemental Figure 8). Together, these data suggest that CSI1 and/or SmaCCs/MASCs are required for the fast recovery of functional CSCs to the PM upon the cessation of stresses such as cellulose inhibition or osmotic stress.

Endocytosis Is Involved in the Formation of Stress-Induced SmaCCs/MASCs

Endocytosis has been postulated to be involved in the recycling of CSCs (Bashline et al., 2014b; Miart et al., 2014). We hypothesize that at least some of the stress-induced SmaCC/MASC-localized CESAs are representative of endocytosed CESAs and that SmaCCs/MASCs are involved in the fast recovery of CSCs to the PM after relief from stress. To investigate whether endocytosis is involved in the formation of SmaCCs/MASCs, we tested whether isoxaben-induced SmaCC/MASC formation is affected by perturbation of endocytosis by pharmacological and genetic means. Wortmannin (Wm) has been previously shown to inhibit the uptake of endocytic markers (Emans et al., 2002; Zhang et al., 2010). We examined FM4-64 internalization upon exposure to Wm in epidermal cells of etiolated hypocotyls. Small intracellular FM4-64 puncta were visible after exposure to FM4-64 in mock treatment (Supplemental Figure 9A). After 4.5 h of exposure to 33 μM Wm, epidermal cells of etiolated seedlings displayed fewer intracellular FM4-64 puncta. Quantification of the internalization of FM4-64 revealed that Wm exhibited an approximate 60% reduction in FM4-64 internalization compared with mock treatment (Supplemental Figure 9B) (Zhang et al., 2010). We also tested whether microtubule organization or dynamics were affected upon exposure to Wm. YFP-TUA5 (a microtubule marker) (Shaw et al., 2003) and EB1b-GFP (a microtubule plus end marker) (Dixit et al., 2006) were used to monitor microtubule organization and microtubule dynamics, respectively. No difference in either microtubule organization or microtubule plus-end dynamics was observed between mock-treated and Wm-treated seedlings (Supplemental Figures 9C and 9D). In addition, Wm treatment did not affect the density of PM-localized CSCs or the coalignment between CSCs and microtubules (Figure 6; Supplemental Movie 8). However, Wm-treated seedlings exhibited an approximate 62% reduction in the accumulation of isoxaben-induced SmaCCs/MASCs compared with mock-treated seedlings (Figures 6B and 6C), suggesting that endocytosis plays a role SmaCC/MASC formation. We previously reported that *ap2m-1* (*μ2-1*) is defective in the endocytosis of CESAs (Bashline et al., 2013). We next examined whether *ap2m-1* (*μ2-1*) affected the accumulation of isoxaben-induced SmaCCs/MASCs. *ap2m-1* (*μ2-1*) exhibited an approximate 44% reduction in the density of isoxaben-induced SmaCCs/MASCs compared with the wild type (Figures 6D to 6F), suggesting that clathrin-mediated endocytosis is involved in the formation of isoxaben-induced SmaCCs/MASCs.

CSI1 and Endocytosis Contribute to the Formation of SmaCCs/MASCs Independently

Since both CSI1 and endocytosis influence the formation of SmaCCs/MASCs, we set out to test whether these two pathways are dependent on one another. To test whether CSI1 is involved in endocytosis, we compared the FM4-64 internalization rate in the wild type and *csi1* mutants. The uptake of FM4-64 was not significantly different in *csi1* mutants (*csi1-3* and *csi1-6*) compared with that in the wild type, suggesting that loss of CSI1 does not affect general endocytosis (Supplemental Figures 10A and 10B).

We next tested whether the inhibition of endocytosis affects the distribution and dynamics of CSI1. A line coexpressing YFP-TUA5 (a microtubule marker) and RFP-CSI1 was treated with 0.1% DMSO (mock) or 33 μM Wm (Supplemental Figure 10C). Wm did not significantly affect the overall distribution pattern of CSI1 at the PM compared with mock treatment. In addition, the velocity of RFP-CSI1 particles was not affected by either mock or Wm

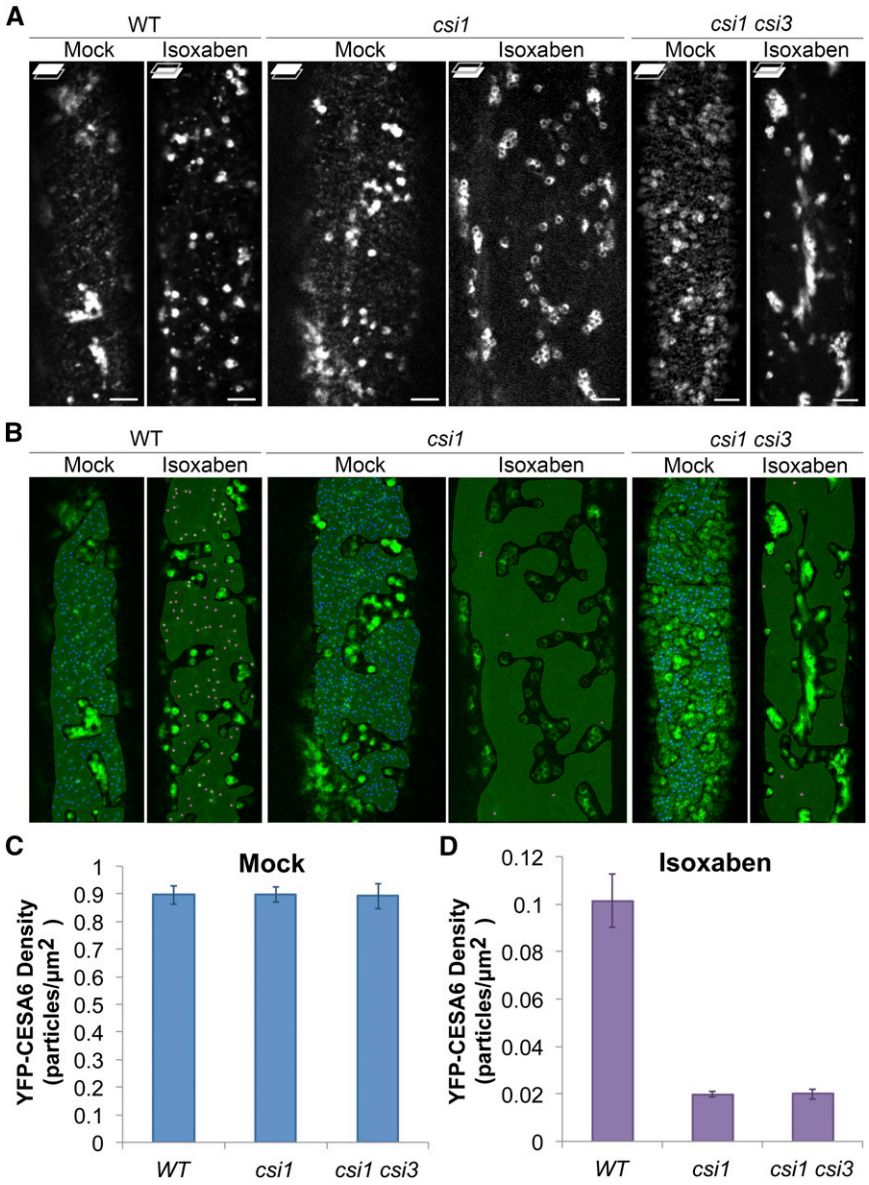

Figure 4. CSI1 Is Required for the Formation of SmaCCs/MASCs.

Arabidopsis seedlings expressing YFP-CESA6 were treated with 0.01% DMSO (mock) or 100 nM isoxaben for 2 h before imaging.
(A) Single optical section sections of YFP-CESA6 in the wild type, *csi1-3*, and *csi1-3 csi3-1* mutants after mock or isoxaben treatment. Focal planes at the PM and lower cell cortex are shown. Bars = 5 μm.
(B) Density analysis of YFP-CESA6 in the wild type, *csi1-3*, and *csi1-3 csi3-1* mutants. A gray mask indicates region of interest lacking the underlying intracellular compartments. Blue or magenta dots represent YFP-CESA6 puncta.
(C) and **(D)** Quantification of YFP-CESA6 at the PM after mock **(C)** or isoxaben **(D)** treatment. $n = \sim$25 to 30 cells from $\sim$15 to 20 individual seedlings in each genetic background after mock or isoxaben treatment. Error bars represent standard errors.

treatment, suggesting that inhibition of endocytosis does not affect the distribution or dynamics of CSI1 (Supplemental Figure 10D). To further investigate whether the association between CSI1 and CESA6 is affected by the inhibition of endocytosis, seedlings coexpressing RFP-CSI1 and GFP-CESA6 were exposed to Wm. RFP-CSI1 and GFP-CESA6 particles extensively overlapped at the PM under both mock and Wm treatment (Supplemental Figure 10E). Together, these data suggest that CSI1 and endocytosis contribute to the formation of SmaCCs/MASCs independently.

DISCUSSION

Cellulose biosynthesis is important for plant growth and development. Therefore, cellulose biosynthesis is tightly regulated in plants by several means. For example, the trafficking of CSCs to

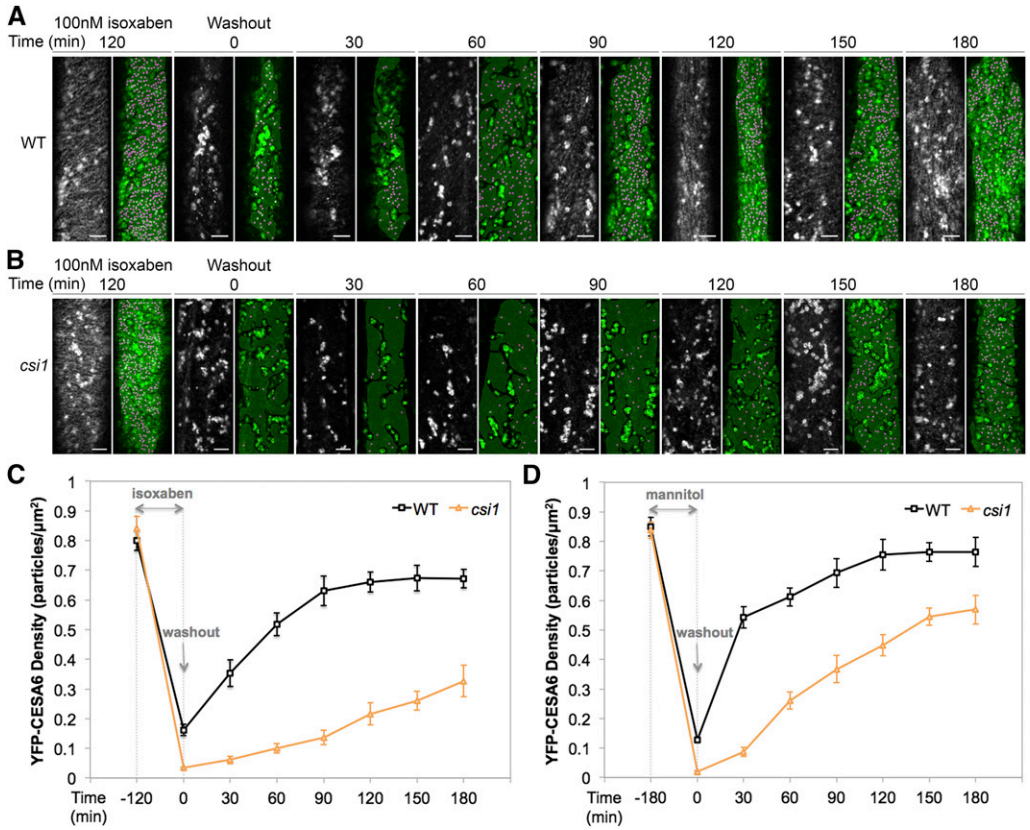

Figure 5. CSI1 Is Required for the Fast Recovery of Plasma Membrane-Localized CSCs after Isoxaben Treatment or Osmotic Stress.

(A) and **(B)** Arabidopsis seedlings expressing YFP-CESA6 in the wild type **(A)** or *csi1-3* **(B)** were imaged before treatment, after treatment with 100 nM isoxaben for 2 h, and at different time points after wash out with liquid 0.5× MS medium. A gray mask indicates region of interest lacking the underlying intracellular compartments. Magenta dots represent YFP-CESA6 puncta. Bars = 5 μm.

(C) Quantification of YFP-CESA6 in the wild type and *csi1-3* after 100 nM isoxaben treatment for 2 h. $n = \sim$15 to 20 cells from ~10 to 15 individual seedlings in each genetic background at different time point. Error bars represent standard errors.

(D) Quantification of YFP-CESA6 density after 200 mM mannitol treatment for 3 h in the wild type and *csi1-3*. $n = \sim$15 to 20 cells from ~10 to 15 individual seedlings in each genetic background at different time point. Error bars represent standard errors.

and from the PM can influence the lifespan, number, and organization of CSCs at the PM and consequentially influence the degree of polymerization, the crystallinity, the orientation, and the total amount of cellulose microfibrils in the cell wall, which may also influence the interaction of cellulose with other wall polymers (Li et al., 2014). The requirement for the vastness of the regulation of cellulose biosynthesis is partly reflected in the wide variety of developmental stages of the plant and in the variety of biotic and abiotic stresses that plants must experience every day. However, the regulatory mechanism of cellulose biosynthesis under abiotic stress has not been well explored. In this study, we showed that CSI1, a component that was previously shown to be essential for linking CSCs to cortical microtubules and for regulating CSC dynamics at the PM, is also important for the formation of SmaCCs/MASCs under stress. Additionally, CSI1-dependent SmaCCs/MASCs are critical for the fast recovery of CSCs to the PM during recovery from isoxaben or osmotic-induced stresses. Thus, CSI1 is a multifunctional protein in the regulation cellulose biosynthesis (Figure 7).

Recycling of the CSC

CSCs are presumably assembled in the Golgi apparatus and then delivered to the PM (Haigler and Brown, 1986). Although delivery of CSCs to the PM has been shown to correlate with the pausing of CSC-containing Golgi bodies at discrete sites on cortical microtubules (Crowell et al., 2009), CSCs have also been documented in Golgi-derived vesicles. After the insertion into the PM, CSCs pause briefly before starting motility at constant velocities, which is indicative of active cellulose synthesis (Crowell et al., 2009; Gutierrez et al., 2009). Presumably active CSCs will terminate at some point and be internalized for degradation or recycling. Although recycling of the CSC is an attractive hypothesis due to the energy cost associated with the degradation of such a large protein complex, there was previously no empirical support for the recycling of PM-localized CSCs. In plants, many proteins have been shown to cycle constantly to and from the PM. Examples of such proteins include the auxin efflux protein PIN-FORMED1, BRASSINOSTEROID RECEPTOR1, L1-specific

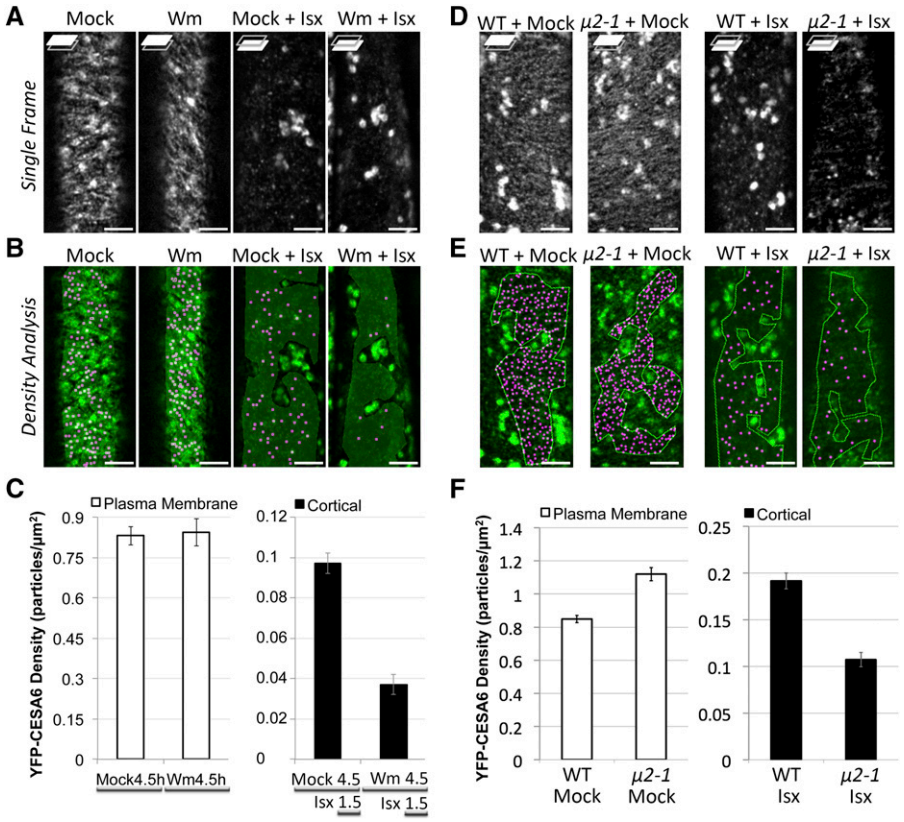

Figure 6. Endocytosis Is Involved in the Formation of SmaCCs/MASCs.

(A) Single optical section of YFP-CESA6 in different treatment as follows: mock (4.5 h), Wm (4.5 h), mock (4.5 h) + Isx (1.5 h), and Wm (4.5 h) + Isx (1.5 h). For Wm (4.5 h) + Isx (1.5 h) treatment, 3-d-old seedlings were pretreated with 33 μM Wm for 3 h and then exposed to a mixture of 33 μM Wm and 100 nM isoxaben (Isx) for 1.5 h. Focal planes at the PM and lower cell cortex are shown. Bars = 5 μm.
(B) Density analysis of single optical section from **(A)**.
(C) Quantification of YFP-CESA6 density. *n* = ~8 to 12 cells from ~5 to 10 individual seedlings in each treatment. Error bars represent standard errors.
(D) Single optical sections of YFP-CESA6 in the wild type or *μ2-1* mutant after 1.5 h of mock treatment or 100 nm isoxaben treatment. Bars = 5 μm.
(E) Density analysis of single optical sections from **(D)**. Shown are representative images from 11 cells from six individual seedlings for each genotype.
(F) Quantification of YFP-CESA6 density. Error bars represent standard errors. *n* = ~8 to 12 cells from ~5 to 10 individual seedlings in each treatment.

receptor kinase ARABIDOPSIS CRINKLY4, the potassium channel KAT1, and the nonactivated flagellin receptor FLS2 (Gifford et al., 2005; Geldner et al., 2007; Sutter et al., 2007; Kitakura et al., 2011; Beck et al., 2012). The recycling of cell wall-synthesizing enzymes at the PM has not previously been confirmed in plants. However, budding yeast have been reported to regulate the turnover of chitin synthase proteins (Chs3p) through a recycling mechanism, and the structure of cellulose is comparable to that of chitin, which is composed of linear chains of *N*-acetylglucosamine, a derivative of glucose (Chuang and Schekman, 1996; Ziman et al., 1996; Ortiz and Novick, 2006). Chs3p cycles between the Golgi apparatus, the early endosome, and the cell surface in response to a cell cycle cue or regulatory responses such as cell wall stress (Santos and Snyder, 1997; Valdivia et al., 2002; Copic et al., 2007). The identification of factors required for Chs3p transport revealed a paradigm of membrane assembly and vesicular trafficking in yeast and mammalian cells (Lesage et al., 2005). While it is impossible to draw meaningful direct parallels about recycling from chitin synthase and cellulose synthase, some of the underlying trafficking machinery is likely conserved between yeast and plants to some extent.

The recycling of cellulose synthase has been proposed to be a potential function of SmaCCs/MASCs (Crowell et al., 2009; Gutierrez et al., 2009; Bashline et al., 2014a; Li et al., 2014). In etiolated Arabidopsis hypocotyls, SmaCCs/MASCs were observed at very low frequency in expanding cells. In addition, it has been difficult to detect SmaCCs/MASCs in elongating cells due to the abundant density of CSCs at the PM, which mask the detection of underlying cortical SmaCCs/MASCs. However, isoxaben treatment or osmotic stress can induce the appearance of SmaCCs/MASCs, since these treatments deplete CSCs from the PM. SmaCCs/MASCs have been hypothesized to originate either from internalized CSCs or from de novo synthesis from the secretion pathway (Crowell et al., 2009; Gutierrez et al., 2009). In the *csi1* null mutant, the secretion of CSCs was not affected (Bringmann et al., 2012). Upon isoxaben treatment, the majority of PM-localized YFP-CESA6 was depleted at the PM in both the wild type and *csi1* mutants. However, SmaCCs/MASC levels were

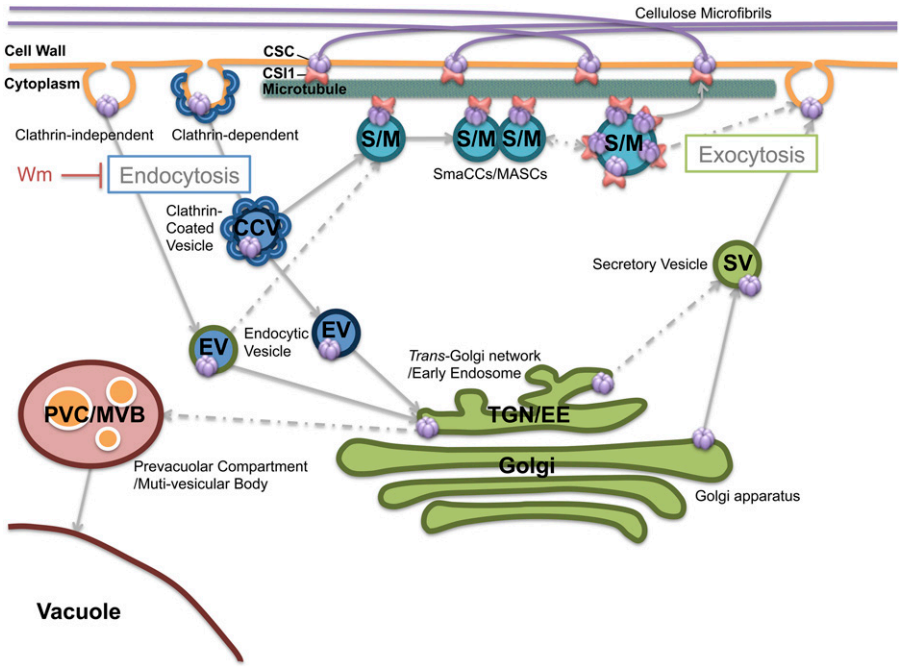

Figure 7. A Snapshot of the Localization and Trafficking Pathways of CSCs.

The CSCs are believed to be assembled in the Golgi apparatus and then secreted to the PM through the TGN/EE. It is largely unknown how secretory vesicles (SV) containing CSCs fuse to the PM, an exocytosis process that may involve actin. Microtubules are involved in docking the secretory vesicle, as SmaCCs/MASCs were often observed to be associated with microtubules. CSI1 mediates the CSC-microtubule interaction. CSCs are internalized through AP2/CME. Newly endocytosed vesicles containing CSCs are predicted to be recycled to the PM through SmaCC-mediated fast recycling and TGN/EE-mediated slow recycling.

significantly reduced in *csi1* under isoxaben treatment. While we cannot rule out the possibility that de novo secretion also supplies some CSCs to SmaCCs/MASCs, the reduced SmaCC/MASC formation in *ap2m* indicates that endocytosis plays a role in the accumulation of SmaCCs/MASCs, which is consistent with reduced SmaCCs/MASCs levels upon Wm treatment. It is tempting to speculate that CESA may have been recycled to the Golgi or TGN/EE for reassembly and delivery or to the vacuole for degradation.

The exact function of SmaCCs/MASCs remains elusive. Here, we propose that SmaCCs/MASCs are required for the fast recycling of CSCs back to the PM during recovery from stresses. The loss of CSI1 in *csi1* mutants caused a reduction in the number of stress-induced SmaCCs/MASCs, which consequentially caused a delay in the recovery of CSCs at the PM after removal of the stress. CSI1-dependent SmaCCs/MASCs might not be essential for CSC recycling. Other slower routes of recycling, perhaps through the Golgi or TGN/EE, might remain intact in *csi1* mutants. However, CSI1-dependent SmaCCs/MASCs might represent an important way for plants to quickly regulate growth under abiotic stress or under normal physiological conditions. In nonelongating epidermal cells such as cells at the basal parts of etiolated hypocotyls, SmaCCs/MASCs are more abundant than in cells undergoing rapid elongation. It remains to be determined whether CSI1 is also required for SmaCC/MASC formation under normal physiological conditions. Overall, our data show that CSI1 plays a critical role in the formation of SmaCCs/MASCs and that SmaCCs/MASCs perform a recycling role during CSC trafficking, at least under stress conditions.

The Involvement of Endocytosis in CSC Recycling

The role of endocytosis has been implicated in cellular responses to abiotic stress. Mitogen-activated protein kinase pathways have been shown to regulate the endocytic pathway under stress conditions in mammalian cells (Cavalli et al., 2001). Similarly, osmotic stress activates distinct mitogen-activated protein kinase pathways in plant cells (Munnik and Meijer, 2001). The small GTPase Rab5 is one of the key regulators of early endocytic events in mammals. The plant homolog of Rab5 can be induced by salt stress and has been shown to function in the endocytic pathway in Arabidopsis (Bolte et al., 2000; Ueda et al., 2001). Although detailed molecular mechanisms linking abiotic stress and endocytosis in plants are lacking, saline or osmotic stress does trigger the activation of endocytic uptake of a biotinylated endocytic marker in rice cells (Bahaji et al., 2003), and overexpression of At-Rab7 increases salt and osmotic stress tolerance, which is consistent with accelerated membrane endocytosis (Mazel et al., 2004). Furthermore, genetic studies have demonstrated the importance of endocytosis for plant fitness under stress (Leshem et al., 2007; Bar et al., 2008a, 2008b; Zwiewka et al., 2015). These observations have led to the hypothesis that plants have developed a more efficient internalization mechanism to retrieve membrane materials to help them adapt to abiotic stress. CSCs may represent

a type of cargo that utilizes this efficient internalization mechanism under abiotic stress.

Our study has shown that SmaCC/MASC formation is dependent on endocytosis. Wm treatment (33 μM 4.5 h) did not affect the PM localization of CSCs in epidermal cells of 3-d-old etiolated hypocotyls. This finding extends observations by Fujimoto et al. (2015), who showed lower concentrations of Wm (4 and 20 μM) deplete GFP-CESA3 from the PM in root epidermal cells of 10-d-old light-grown Arabidopsis seedlings. The discrepancy may be attributed to differences in Wm treatments, systems, and/or growth conditions. The reduction of SmaCCs/MASCs accumulation by pharmacological (Wm) or genetic methods (*ap2m-1*) suggests CME-mediated endocytosis is involved in the formation of SmaCCs/MASCs. However, SmaCCs/MASCs were not completely depleted in *ap2m-1* (*μ2-1*), suggesting that CME may not be the only mechanism for CSC internalization under stress. Alternatively, CME may function through an AP2-independent pathway such as through the TPLATE complex, which has recently been identified as an alternative CME adaptor complex (Van Damme et al., 2011; Gadeyne et al., 2014). It remains to be tested whether TPLATE is involved in SmaCC/MASC formation.

Internalized CESAs can presumably be trafficked to one of three different destinations: SmaCCs/MASCs for endocytic recycling, the Golgi or TGN/EE for reassembly and delivery, or the vacuole for degradation. CESAs have been observed at the PM, in the Golgi, TGN/EE, and SmaCCs/MASCs, whereas CSI1 has only been observed at the PM and in SmaCCs/MASCs (Crowell et al., 2009; Gutierrez et al., 2009). Unlike CESA, which is an integral membrane protein, CSI1 is a peripheral protein. Therefore, it is unlikely that CSI1 is internalized together with CESA during endocytosis. Without CSI1, *csi1* mutants exhibited normal endocytosis of FM4-64 dye, but could not form SmaCCs/MASCs. Therefore, the association of CSI1 with SmaCCs/MASCs likely occurs after the endocytosis of CESAs and before the recycling of CESAs back to the PM, but it remains to be determined how CSI1 is involved in SmaCC/MASC formation. Does it occur immediately after CSC internalization or after CSC-containing vesicles have been sorted through the TGN/EE? Further studies are required to determine the specific trafficking route involved in the association of CSI1 with SmaCCs/MASCs.

The Role of CSI1 and Microtubules in Fast CSC Recovery after Stress

SmaCCs/MASCs were often observed to colocalize with microtubules, and microtubules are necessary for the cortical tethering of SmaCCs/MASCs (Gutierrez et al., 2009). However, the mechanism underlying microtubule-dependent SmaCC/MASC formation is unknown. Our data indicate that in addition to requiring microtubules (Gutierrez et al., 2009), SmaCC/MASC formation is also dependent on CSI1. Interestingly, the C-terminal C2 domain of CSI1 is sufficient for the recruitment of CSI1 to SmaCCs/MASCs but not for the association of CSI1 with PM-localized CSCs. The C-terminal C2 domain of CSI1 is also important for microtubule binding in vitro and in vivo. These data support a functional connection between microtubules and CSI1 in the formation of SmaCCs/MASCs. Presumably, cortical microtubules act as a landmark for CSC delivery and insertion to the PM. This is consistent with the previous observations that SmaCCs/MASCs are substantially associated with microtubules, Golgi bodies pause on microtubules before delivery, and CSCs were observed to appear along microtubules during delivery events after photobleaching (Crowell et al., 2009; Gutierrez et al., 2009). After insertion, CSCs have been observed to pause briefly before they move along microtubules in the presence of CSI1. However, neither general endocytosis nor CSC delivery to the PM is affected in *csi1* or by the depletion of microtubules. It appears that the requirement of both microtubules and CSI1 is specific for SmaCC/MASC formation. It remains to be determined how microtubules affect SmaCC/MASC formation. A recent study showed that microtubules influence the resident lifespan and mobility of dynamin and clathrin light chain (Konopka et al., 2008). It remains to be determined whether SmaCC/MASC formation is dependent on CME through a microtubule-related function. Alternatively, cortical microtubules might be involved in efficiently retaining, sorting, and/or transporting internalized CSC-containing vesicles. Identification of the molecular players involved in the sorting and recycling processes will greatly advance our understanding of CSC trafficking.

METHODS

Plant Materials and Growth Conditions

Arabidopsis thaliana seeds were surface sterilized using 30% bleach, stratified at 4°C for 3 d, plated on MS plates (0.5× MS salts, 0.8% agar, and 0.05% MES, pH 5.7), and grown vertically at 22°C in darkness for 2 to 3 d before drug treatment and imaging.

Mutants and Transgenic Lines

Seeds of *csi1-3* (SALK_138584), *csi1-6* (SALK_051146), and *csi3-1* (GABI_308G07) were obtained from the Arabidopsis Biological Resource Center at Ohio State University. The identification of homozygous lines was described previously (Gu et al., 2010; Lei et al., 2013). Homozygous YFP-CESA6 *prc1-1* seeds (line A6Y-11) were obtained from Chris Somerville (Energy Bioscience Institute, University of California). Homozygous mCherry-CESA6 *prc1-1* transgenic lines were described previously (Bashline et al., 2013). To construct the proCSI1:RFP-CSI1$^{1\text{-}2013}$ line, a 35S promoter in pH7RWG2 (Karimi et al., 2002) was replaced with the 3-kb *CSI1* promoter using primers flanking *Sac*I and *Spec*I sites (Supplemental Table 2). The sequence of CSI1$^{1\text{-}2013}$ was PCR amplified (Supplemental Table 2) and cloned into *pDONR/zeo* vector (Life Technologies). pH7RWG2-proCSI1:CSI1$^{1\text{-}2013}$ was then generated using Gateway technology between pH7RWG2-proCSI1 and pDONR/zeo-CSI1$^{1\text{-}2013}$. The verified construct was transformed into *csi1-6* by *Agrobacterium tumefaciens*-mediated transformation (Clough and Bent., 1998). Various YFP-CSI1 truncations were generated by Gateway technology between pEarley104 and pDONR/zeo using similar methods as described for ProCSI1: CSI1$^{1\text{-}2013}$. Briefly, CSI1 truncations were PCR amplified (Supplemental Table 2) and introduced into pDONR/zeo using Gateway BP Clonase. pEarley104-CSI1^{truncations} were then generated between pEarley104 and pDONR/zeo-CSI1^{truncations} using Gateway LR Clonase II. The verified constructs were transformed into Columbia-0 by Agrobacterium-mediated transformation. T2 homozygous lines were selected for confocal microscopy analysis.

Live-Cell Imaging

The hypocotyls of 3-d-old etiolated seedlings were used for live-cell imaging. Imaging was performed on a Yokogawa CSUX1spinning disk

system as described previously (Gu et al., 2010; Bashline et al., 2013). Image analysis was performed using Metamorph (Molecular Devices), ImageJ software (version 1.43u; http://rsbweb.nih.gov/ij/), and Imaris (Bitplane) software. CESA particle density measurements and CESA particle dynamics analysis were performed as described previously (Gu et al., 2010; Bashline et al., 2013).

FM4-64 Internalization Assay

FM4-64 internalization in *csi1* mutants was observed and analyzed as described previously (Bashline et al., 2013). For roots cells, the exposure of FM4-64 was 10 min. FM4-64 internalization after Wm treatment was observed in the epidermal cells of 3-d-old etiolated hypocotyls. Due to the relative thick cell wall of these cells, the FM4-64 incubation time was extended to 20 min.

Drug Treatments

For live-cell imaging, 2.5-d-old etiolated seedlings were submerged in MS liquid medium containing the drug and incubated in darkness for variable lengths of time. Isoxaben and Wm were prepared as stock solutions at 50 and 33 mM, respectively, in DMSO. For oryzalin, a stock solution was prepared at 50 mM. Stock solutions were diluted using MS liquid medium immediately before each experiment. For mock treatment, seedlings were incubated in diluted DMSO solution.

Protein Expression and in Vitro Pull-Down Assay

Various CSI1 truncations were amplified using PCR primers (Supplemental Table 2) and subcloned into YG201 (Bashline et al., 2013), which provides a His tag protein fusion. The expression and purification of CSI1 truncations were performed as described previously. Purification of GST-CESA1CD and GST1-CESA3CD was described previously (Lei et al., 2014). The in vitro pull-down assay was performed as described previously (Bashline et al., 2013).

Immunoblot Analysis

Proteins were separated by SDS-PAGE and transferred to nitrocellulose membranes. Immunoblotting was performed by blocking the nitrocellulose membrane with Tris-buffered saline and 0.1% Tween 20 (TBS-T) containing 5% nonfat milk, followed by incubation for 2 h at room temperature with the horseradish peroxidase-conjugated His antibody diluted 1:5000. After extensive washing with TBS-T, His fusion proteins were detected on a blue sensitive film (Cystalgen) by chemiluminescence using a horseradish peroxidase-conjugated His antibody and SuperSignal West Femto substrate (Thermo).

In Vitro Microtubule Binding Assay

The in vitro microtubule binding assay was performed according to the manufacturer's instructions (Cytoskeleton) as described previously (Li et al., 2012). Briefly, microtubules were polymerized in vitro and stabilized by taxol. Approximately 10 μg taxol-stabilized microtubules was mixed with MAP2 (positive control), BSA (negative control), and affinity-purified His-tagged CSI1 truncations. After incubation of proteins with or without microtubules, samples were centrifuged, and proteins present in pellet or supernatant were analyzed by SDS/PAGE and visualized by Coomassie Brilliant Blue staining.

For measurement of binding affinity, increasing amounts of taxol-stabilized tubulin were incubated with 1 μM purified CSI1$^{2012\text{-}2150}$ truncation for 30 min at room temperature. After centrifugation, 25% (8 μL out of 32 μL total volume) of each pellet was resolved by SDS-PAGE and visualized by Coomassie Brilliant Blue staining. Protein gels were scanned and the total signal intensity was quantified using commercial software (GeneTools; Syngene). The dissociation constant (K_d) for CSI1$^{2012\text{-}2150}$ binding to taxol-stabilized microtubules was determined by best fit to the data according to the equation: $q = (q_{max} \times c)/(K_d + c)$.

Modeling

The secondary structure of CSI1, consisting of 2150 amino acids (AT2g22125), was predicted using PSIPRED (Jones, 1999). Based on secondary structure prediction, the CSI1 protein consists of many α-helices with the exception of the C2 domain, which is folded into β-sheets. The 3D structure prediction was performed using RaptorX (Källberg et al., 2012). RaptorX is a template-based protein prediction server that uses multiple distantly related template proteins and a nonlinear scoring function with a probabilistic consistency algorithm. RaptorX was chosen because it was designed for structural prediction of proteins with low sequence homology. The 2150-amino acid sequence was separated into three domains for 3D structure prediction: part 1 (residues 1 to 648), part 2 (residues 649 to 1170), and part 3 (residues 1171 to 2150). The 3D structure prediction was based on 19 models (Supplemental Table 1). The structures were assembled using Accelrys Discovery Studio Visualizer (http://accelrys.com/products/discovery-studio) into a 2150-amino acid model of CSI1 protein and refined with all-atom MD simulations. CSI1 protein was solvated explicitly using a TIP3 water box. CSI2, together with water and ions (Na^+ and Cl^-), add up to a system composed of 220,909 atoms. The initial configurations of the whole system were minimized using 1000 cycles of steepest descent and conjugate gradient. The system was gradually heated to 300K, and the equilibration MD and production runs were performed using AMBER 14 (Langevin dynamics with the NPT ensemble with a relaxation time of 1.0 ps, with a collision frequency of 1.0) and the ff14SB force field (Hornak et al., 2006). The SHAKE algorithm allowed for a 2.0-fs time step. The Particle-Mesh Ewald method was used to treat all electrostatic interactions with a cutoff of 10 Å.

Accession Numbers

Sequence data from this article can be found in the Arabidopsis Genome Initiative or GenBank/EMBL databases under the following accession numbers: At2g22125 (CSI1), At1g77460 (CSI3), At5g05170 (CESA3), and At5g64740 (CESA6).

Supplemental Data

Supplemental Figure 1. Microtubule binding assay of CSI1$^{2012\text{-}2150}$.

Supplemental Figure 2. CSI1 binds to CESA through multiple binding sites in vitro.

Supplemental Figure 3. Subcellular localization of C-terminal CSI1 truncations.

Supplemental Figure 4. The C2 domain of CSI1 is indispensable for the function of CSI1.

Supplemental Figure 5. Sequence used for RaptorX prediction and secondary structure prediction from PRESIPED server.

Supplemental Figure 6. Structure of CSI1 refined with MD simulations.

Supplemental Figure 7. CSI3 is not required for accumulation of SmaCCs.

Supplemental Figure 8. CSI1 is required for fast recovery of plasma membrane-localized CSCs after osmotic stress.

Supplemental Figure 9. Wortmannin treatment delays internalization of FM4-64, but it does not affect the organization and dynamics of microtubules.

Supplemental Figure 10. CSI1 and endocytosis contribute to the formation of SmaCCs independently.

Supplemental Table 1. Representative models that were generated by RaptorX server.

Supplemental Table 2. DNA primers used in this study.

Supplemental Movie 1. YFP-CSI1$^{1738-2150}$ localizes at plasma membrane excluded from underlying microtubules.

Supplemental Movie 2. YFP-CSI1$^{2012-2150}$ colocalizes with cortical microtubules.

Supplemental Movie 3. YFP-CSI1$^{2012-2150}$ localization is dependent on microtubules.

Supplemental Movie 4. Majority of YFP-CSI1$^{2012-2150}$-associated SmaCCs are immobile.

Supplemental Movie 5. YFP-CSI1$^{2012-2150}$ tracks microtubule-shrinking ends.

Supplemental Movie 6. YFP-CSI1$^{2012-2150}$ comigrates with SmaCCs.

Supplemental Movie 7. CSI1 is required for accumulation of SmaCCs.

Supplemental Movie 8. Wortmannin inhibits the accumulation of SmaCCs.

ACKNOWLEDGMENTS

We thank Ryan Gutierrez and David Ehrhardt for providing the mCherry-TUA5 GV3101 strain and CFP-TUA1 and YFP-TUA5 transgenic lines. We thank Richard Cyr for providing EB1b-GFP transgenic lines. Y.G. and L.L. were supported by the National Science Foundation (Grant 1121375). L.B. and S.L. were supported by the Department of Biochemistry and Molecular Biology, Pennsylvania State University. Y.G.Y. and A.S. were supported by The Center for LignoCellulose Structure and Formation, an Energy Frontier Research Center funded by the DOE, Office of Science, BES under Award DE-SC0001090.

AUTHOR CONTRIBUTIONS

L.L., S.L., and Y.G. designed research. L.L., A.S., S.L., L.B., and Y.G. performed research. L.L., S.L., L.B., A.S., Y.G.Y., and Y.G. analyzed data. L.L., S.L., L.B., A.S., Y.G.Y., and Y.G. wrote the article.

Received May 18, 2015; revised September 14, 2015; accepted September 22, 2015; published October 6, 2015.

REFERENCES

Albertson, R., Riggs, B., and Sullivan, W. (2005). Membrane traffic: a driving force in cytokinesis. Trends Cell Biol. **15:** 92–101.

Bahaji, A., Aniento, F., and Cornejo, M.J. (2003). Uptake of an endocytic marker by rice cells: variations related to osmotic and saline stress. Plant Cell Physiol. **44:** 1100–1111.

Bar, M., Aharon, M., Benjamin, S., Rotblat, B., Horowitz, M., and Avni, A. (2008b). AtEHDs, novel Arabidopsis EH-domain-containing proteins involved in endocytosis. Plant J. **55:** 1025–1038.

Bar, M., Benjamin, S., Horowitz, M., and Avni, A. (2008a). AtEHDs in endocytosis. Plant Signal. Behav. **3:** 1008–1010.

Bashline, L., Li, S., and Gu, Y. (2014a). The trafficking of the cellulose synthase complex in higher plants. Ann. Bot. (Lond.) **114:** 1059–1067.

Bashline, L., Lei, L., Li, S., and Gu, Y. (2014b). Cell wall, cytoskeleton, and cell expansion in higher plants. Mol. Plant **7:** 586–600.

Bashline, L., Li, S., Anderson, C.T., Lei, L., and Gu, Y. (2013). The endocytosis of cellulose synthase in Arabidopsis is dependent on μ2, a clathrin-mediated endocytosis adaptin. Plant Physiol. **163:** 150–160.

Beck, M., Zhou, J., Faulkner, C., MacLean, D., and Robatzek, S. (2012). Spatio-temporal cellular dynamics of the Arabidopsis flagellin receptor reveal activation status-dependent endosomal sorting. Plant Cell **24:** 4205–4219.

Bolte, S., Schiene, K., and Dietz, K.J. (2000). Characterization of a small GTP-binding protein of the rab 5 family in *Mesembryanthemum crystallinum* with increased level of expression during early salt stress. Plant Mol. Biol. **42:** 923–936.

Bolte, S., Talbot, C., Boutte, Y., Catrice, O., Read, N.D., and Satiat-Jeunemaitre, B. (2004). FM-dyes as experimental probes for dissecting vesicle trafficking in living plant cells. J. Microsc. **214:** 159–173.

Bringmann, M., Li, E., Sampathkumar, A., Kocabek, T., Hauser, M.T., and Persson, S. (2012). POM-POM2/cellulose synthase interacting1 is essential for the functional association of cellulose synthase and microtubules in Arabidopsis. Plant Cell **24:** 163–177.

Cavalli, V., Vilbois, F., Corti, M., Marcote, M.J., Tamura, K., Karin, M., Arkinstall, S., and Gruenberg, J. (2001). The stress-induced MAP kinase p38 regulates endocytic trafficking via the GDI:Rab5 complex. Mol. Cell **7:** 421–432.

Chalmers, A.D., and Whitley, P. (2012). Continuous endocytic recycling of tight junction proteins: how and why? Essays Biochem. **53:** 41–54.

Chuang, J.S., and Schekman, R.W. (1996). Differential trafficking and timed localization of two chitin synthase proteins, Chs2p and Chs3p. J. Cell Biol. **135:** 597–610.

Clough, S.J., and Bent, A.F. (1998). Floral dip: a simplified method for Agrobacterium-mediated transformation of *Arabidopsis thaliana*. Plant J. **16:** 735–743.

Cocucci, E., Aguet, F., Boulant, S., and Kirchhausen, T. (2012). The first five seconds in the life of a clathrin-coated pit. Cell **150:** 495–507.

Collings, D.A., Gebbie, L.K., Howles, P.A., Hurley, U.A., Birch, R.J., Cork, A.H., Hocart, C.H., Arioli, T., and Williamson, R.E. (2008). Arabidopsis dynamin-like protein DRP1A: a null mutant with widespread defects in endocytosis, cellulose synthesis, cytokinesis, and cell expansion. J. Exp. Bot. **59:** 361–376.

Copic, A., Starr, T.L., and Schekman, R. (2007). Ent3p and Ent5p exhibit cargo-specific functions in trafficking proteins between the trans-Golgi network and the endosomes in yeast. Mol. Biol. Cell **18:** 1803–1815.

Crowell, E.F., Bischoff, V., Desprez, T., Rolland, A., Stierhof, Y.D., Schumacher, K., Gonneau, M., Höfte, H., and Vernhettes, S. (2009). Pausing of Golgi bodies on microtubules regulates secretion of cellulose synthase complexes in Arabidopsis. Plant Cell **21:** 1141–1154.

Di Rubbo, S., et al. (2013). The clathrin adaptor complex AP-2 mediates endocytosis of brassinosteroid insensitive1 in Arabidopsis. Plant Cell **25:** 2986–2997.

Dixit, R., Chang, E., and Cyr, R. (2006). Establishment of polarity during organization of the acentrosomal plant cortical microtubule array. Mol. Biol. Cell **17:** 1298–1305.

Drakakaki, G., van de Ven, W., Pan, S., Miao, Y., Wang, J., Keinath, N.F., Weatherly, B., Jiang, L., Schumacher, K., Hicks, G., and Raikhel, N. (2012). Isolation and proteomic analysis of the SYP61 compartment reveal its role in exocytic trafficking in Arabidopsis. Cell Res. **22:** 413–424.

Eaton, S., and Martin-Belmonte, F. (2014). Cargo sorting in the endocytic pathway: a key regulator of cell polarity and tissue dynamics. Cold Spring Harb. Perspect. Biol. **6:** a016899.

Emans, N., Zimmermann, S., and Fischer, R. (2002). Uptake of a fluorescent marker in plant cells is sensitive to brefeldin A and wortmannin. Plant Cell **14:** 71–86.

Fan, L., Hao, H., Xue, Y., Zhang, L., Song, K., Ding, Z., Botella, M.A., Wang, H., and Lin, J. (2013). Dynamic analysis of Arabidopsis AP2 σ subunit reveals a key role in clathrin-mediated endocytosis and plant development. Development **140:** 3826–3837.

Fujimoto, M., Suda, Y., Vernhettes, S., Nakano, A., and Ueda, T. (2015). Phosphatidylinositol 3-kinase and 4-kinase have distinct roles in intracellular trafficking of cellulose synthase complexes in *Arabidopsis thaliana*. Plant Cell Physiol. **56:** 287–298.

Gadeyne, A., et al. (2014). The TPLATE adaptor complex drives clathrin-mediated endocytosis in plants. Cell **156:** 691–704.

Geldner, N., Hyman, D.L., Wang, X., Schumacher, K., and Chory, J. (2007). Endosomal signaling of plant steroid receptor kinase BRI1. Genes Dev. **21:** 1598–1602.

Gifford, M.L., Robertson, F.C., Soares, D.C., and Ingram, G.C. (2005). ARABIDOPSIS CRINKLY4 function, internalization, and turnover are dependent on the extracellular crinkly repeat domain. Plant Cell **17:** 1154–1166.

Gu, Y., Kaplinsky, N., Bringmann, M., Cobb, A., Carroll, A., Sampathkumar, A., Baskin, T.I., Persson, S., and Somerville, C.R. (2010). Identification of a cellulose synthase-associated protein required for cellulose biosynthesis. Proc. Natl. Acad. Sci. USA **107:** 12866–12871.

Gutierrez, R., Lindeboom, J.J., Paredez, A.R., Emons, A.M., and Ehrhardt, D.W. (2009). Arabidopsis cortical microtubules position cellulose synthase delivery to the plasma membrane and interact with cellulose synthase trafficking compartments. Nat. Cell Biol. **11:** 797–806.

Haigler, C.H., and Brown, R.M. (1986). Transport of rosettes from the Golgi apparatus to the plasma membrane in isolated mesophyll cells of *Zinnia elegans* during differentiation to tracheary elements in suspension culture. Protoplasma **134:** 111–120.

Hornak, V., Abel, R., Okur, A., Strockbine, B., Roitberg, A., and Simmerling, C. (2006). Comparison of multiple Amber force fields and development of improved protein backbone parameters. Proteins **65:** 712–725.

Ito, E., Fujimoto, M., Ebine, K., Uemura, T., Ueda, T., and Nakano, A. (2012). Dynamic behavior of clathrin in *Arabidopsis thaliana* unveiled by live imaging. Plant J. **69:** 204–216.

Jackson, L.P., Kelly, B.T., McCoy, A.J., Gaffry, T., James, L.C., Collins, B.M., Höning, S., Evans, P.R., and Owen, D.J. (2010). A large-scale conformational change couples membrane recruitment to cargo binding in the AP2 clathrin adaptor complex. Cell **141:** 1220–1229.

Jones, D.T. (1999). Protein secondary structure prediction based on position-specific scoring matrices. J. Mol. Biol. **292:** 195–202.

Källberg, M., Wang, H., Wang, S., Peng, J., Wang, Z., Lu, H., and Xu, J. (2012). Template-based protein structure modeling using the RaptorX web server. Nat. Protoc. **7:** 1511–1522.

Karimi, M., Inzé, D., and Depicker, A. (2002). Gateway vectors for Agrobacterium-mediated plant transformation. Trends Plant Sci. **7:** 193–195.

Kim, S.Y., Xu, Z.Y., Song, K., Kim, D.H., Kang, H., Reichardt, I., Sohn, E.J., Friml, J., Juergens, G., and Hwang, I. (2013). Adaptor protein complex 2-mediated endocytosis is crucial for male reproductive organ development in Arabidopsis. Plant Cell **25:** 2970–2985.

Kitakura, S., Vanneste, S., Robert, S., Löfke, C., Teichmann, T., Tanaka, H., and Friml, J. (2011). Clathrin mediates endocytosis and polar distribution of PIN auxin transporters in Arabidopsis. Plant Cell **23:** 1920–1931.

Konopka, C.A., Backues, S.K., and Bednarek, S.Y. (2008). Dynamics of Arabidopsis dynamin-related protein 1C and a clathrin light chain at the plasma membrane. Plant Cell **20:** 1363–1380.

Lei, L., Li, S., Du, J., Bashline, L., and Gu, Y. (2013). CELLULOSE SYNTHASE INTERACTIVE3 regulates cellulose biosynthesis in both a microtubule-dependent and microtubule-independent manner in *Arabidopsis*. Plant Cell **25:** 4912–4923.

Lei, L., Li, S., and Gu, Y. (2012). Cellulose synthase interactive protein 1 (CSI1) mediates the intimate relationship between cellulose microfibrils and cortical microtubules. Plant Signal. Behav. **7:** 714–718.

Lei, L., Zhang, T., Strasser, R., Lee, C.M., Gonneau, M., Mach, L., Vernhettes, S., Kim, S.H., J Cosgrove, D., Li, S., and Gu, Y. (2014). The jiaoyao1 mutant is an allele of korrigan1 that abolishes endoglucanase activity and affects the organization of both cellulose microfibrils and microtubules in Arabidopsis. Plant Cell **26:** 2601–2616.

Lesage, G., Shapiro, J., Specht, C.A., Sdicu, A.M., Ménard, P., Hussein, S., Tong, A.H., Boone, C., and Bussey, H. (2005). An interactional network of genes involved in chitin synthesis in *Saccharomyces cerevisiae*. BMC Genet. **6:** 8.

Leshem, Y., Seri, L., and Levine, A. (2007). Induction of phosphatidylinositol 3-kinase-mediated endocytosis by salt stress leads to intracellular production of reactive oxygen species and salt tolerance. Plant J. **51:** 185–197.

Li, S., Bashline, L., Lei, L., and Gu, Y. (2014). Cellulose synthesis and its regulation. Arabidopsis Book **12:** e0169.

Li, S., Lei, L., Somerville, C.R., and Gu, Y. (2012). Cellulose synthase interactive protein 1 (CSI1) links microtubules and cellulose synthase complexes. Proc. Natl. Acad. Sci. USA **109:** 185–190.

Mazel, A., Leshem, Y., Tiwari, B.S., and Levine, A. (2004). Induction of salt and osmotic stress tolerance by overexpression of an intracellular vesicle trafficking protein AtRab7 (AtRabG3e). Plant Physiol. **134:** 118–128.

Miart, F., Desprez, T., Biot, E., Morin, H., Belcram, K., Höfte, H., Gonneau, M., and Vernhettes, S. (2014). Spatio-temporal analysis of cellulose synthesis during cell plate formation in Arabidopsis. Plant J. **77:** 71–84.

Munnik, T., and Meijer, H.J. (2001). Osmotic stress activates distinct lipid and MAPK signalling pathways in plants. FEBS Lett. **498:** 172–178.

Ortiz, D., and Novick, P.J. (2006). Ypt32p regulates the translocation of Chs3p from an internal pool to the plasma membrane. Eur. J. Cell Biol. **85:** 107–116.

Paredez, A.R., Somerville, C.R., and Ehrhardt, D.W. (2006). Visualization of cellulose synthase demonstrates functional association with microtubules. Science **312:** 1491–1495.

Samaj, J., Read, N.D., Volkmann, D., Menzel, D., and Baluska, F. (2005). The endocytic network in plants. Trends Cell Biol. **15:** 425–433.

Santos, B., and Snyder, M. (1997). Targeting of chitin synthase 3 to polarized growth sites in yeast requires Chs5p and Myo2p. J. Cell Biol. **136:** 95–110.

Sethaphong, L., Haigler, C.H., Kubicki, J.D., Zimmer, J., Bonetta, D., DeBolt, S., and Yingling, Y.G. (2013). Tertiary model of a plant cellulose synthase. Proc. Natl. Acad. Sci. USA **110:** 7512–7517.

Shaw, S.L., Kamyar, R., and Ehrhardt, D.W. (2003). Sustained microtubule treadmilling in Arabidopsis cortical arrays. Science **300:** 1715–1718.

Somerville, C. (2006). Cellulose synthesis in higher plants. Annu. Rev. Cell Dev. Biol. **22:** 53–78.

Song, K., Jang, M., Kim, S.Y., Lee, G., Lee, G.J., Kim, D.H., Lee, Y., Cho, W., and Hwang, I. (2012). An A/ENTH domain-containing

protein functions as an adaptor for clathrin-coated vesicles on the growing cell plate in Arabidopsis root cells. Plant Physiol. **159:** 1013–1025.

Steinman, R.M., Mellman, I.S., Muller, W.A., and Cohn, Z.A. (1983). Endocytosis and the recycling of plasma membrane. J. Cell Biol. **96:** 1–27.

Sutter, J.U., Sieben, C., Hartel, A., Eisenach, C., Thiel, G., and Blatt, M.R. (2007). Abscisic acid triggers the endocytosis of the Arabidopsis KAT1 K+ channel and its recycling to the plasma membrane. Curr. Biol. **17:** 1396–1402.

Ueda, T., Yamaguchi, M., Uchimiya, H., and Nakano, A. (2001). Ara6, a plant-unique novel type Rab GTPase, functions in the endocytic pathway of *Arabidopsis thaliana*. EMBO J. **20:** 4730–4741.

Valdivia, R.H., Baggott, D., Chuang, J.S., and Schekman, R.W. (2002). The yeast clathrin adaptor protein complex 1 is required for the efficient retention of a subset of late Golgi membrane proteins. Dev. Cell **2:** 283–294.

Van Damme, D., Gadeyne, A., Vanstraelen, M., Inzé, D., Van Montagu, M.C., De Jaeger, G., Russinova, E., and Geelen, D. (2011). Adaptin-like protein TPLATE and clathrin recruitment during plant somatic cytokinesis occurs via two distinct pathways. Proc. Natl. Acad. Sci. USA **108:** 615–620.

Viotti, C., et al. (2010). Endocytic and secretory traffic in Arabidopsis merge in the trans-Golgi network/early endosome, an independent and highly dynamic organelle. Plant Cell **22:** 1344–1357.

Wang, C., Yan, X., Chen, Q., Jiang, N., Fu, W., Ma, B., Liu, J., Li, C., Bednarek, S.Y., and Pan, J. (2013). Clathrin light chains regulate clathrin-mediated trafficking, auxin signaling, and development in Arabidopsis. Plant Cell **25:** 499–516.

Wickström, S.A., and Fässler, R. (2011). Regulation of membrane traffic by integrin signaling. Trends Cell Biol. **21:** 266–273.

Worden, N., Park, E., and Drakakaki, G. (2012). Trans-Golgi network: an intersection of trafficking cell wall components. J. Integr. Plant Biol. **54:** 875–886.

Xiong, G., Li, R., Qian, Q., Song, X., Liu, X., Yu, Y., Zeng, D., Wan, J., Li, J., and Zhou, Y. (2010). The rice dynamin-related protein DRP2B mediates membrane trafficking, and thereby plays a critical role in secondary cell wall cellulose biosynthesis. Plant J. **64:** 56–70.

Yamaoka, S., Shimono, Y., Shirakawa, M., Fukao, Y., Kawase, T., Hatsugai, N., Tamura, K., Shimada, T., and Hara-Nishimura, I. (2013). Identification and dynamics of Arabidopsis adaptor protein-2 complex and its involvement in floral organ development. Plant Cell **25:** 2958–2969.

Zhang, Y., He, J., Lee, D., and McCormick, S. (2010). Interdependence of endomembrane trafficking and actin dynamics during polarized growth of Arabidopsis pollen tubes. Plant Physiol. **152:** 2200–2210.

Ziman, M., Chuang, J.S., and Schekman, R.W. (1996). Chs1p and Chs3p, two proteins involved in chitin synthesis, populate a compartment of the *Saccharomyces cerevisiae* endocytic pathway. Mol. Biol. Cell **7:** 1909–1919.

Zwiewka, M., Nodzyński, T., Robert, S., Vanneste, S., and Friml, J. (2015). Osmotic stress modulates the balance between exocytosis and clathrin-mediated endocytosis in *Arabidopsis thaliana*. Mol. Plant **8:** 1175–1187.